

Variational Monte Carlo for Interacting Electrons in Quantum Dots

Ari Harju

*Laboratory of Physics, Helsinki University of Technology,
P.O. Box 1100, FIN-02015 HUT, Finland*

We use a variational Monte Carlo algorithm to solve the electronic structure of two-dimensional semiconductor quantum dots in external magnetic field. We present accurate many-body wave functions for the system in various magnetic field regimes. We show the importance of symmetry, and demonstrate how it can be used to simplify the variational wave functions. We present in detail the algorithm for efficient wave function optimization. We also present a Monte Carlo -based diagonalization technique to solve the quantum dot problem in the strong magnetic field limit where the system is of a multiconfiguration nature.

PACS numbers: 71.10.-w, 73.21.La, 02.70.Ss

1. INTRODUCTION

The nanoscale semiconductor systems are technically very promising for future components of microelectronic devices. From theoretical point of view, quantum dot (QD) systems are a valuable source of novel quantum effects. Many of these result from the fact that the electron-electron interaction and external magnetic field have greatly enhanced effects compared to atoms and molecules. This raises new challenges for the theoretical methods, and the validity of approximations in, e.g., mean-field approaches (See Ref. 1 for a review) can be questioned. For this reason, QD systems serve as perfect test cases to develop electronic structure methods, with the results applicable to a great variety of physical problems where mean-field approaches have been used. In addition, many of the system parameters are tunable, e.g., the electron number in QDs can be changed one by one and the confinement potential can be varied by external gates.

The quantum Monte Carlo (QMC) methods are among the most accu-

A. Harju

rate ones for tackling a problem of interacting quantum particles². Often the simplest QMC method, namely the variational QMC (VMC), is able to reveal the most important correlation effects. In many quantum systems, further accuracy in, e.g., energy is needed, and in these cases methods such as the diffusion QMC (DMC) allow one to obtain more accurate estimates for various observables. Even DMC is still not always exact. For fermions, the standard application of the DMC is variational *with the given nodes*. In finite magnetic fields, the fixed-node method is generalized to a fixed-phase one, being again variational³. The ground-state wave function of a bosonic system (in zero magnetic field) does not have nodes in the ground state, and DMC has only statistical error in the observables. For finite magnetic fields, the bosonic problem has a non-trivial phase structure, and also in that case a fixed-phase strategy has to be used.

2. MODEL AND METHODS

2.1. Model for Quantum Dots

The generally used model Hamiltonian of an N -electron QD system can be written as

$$\mathcal{H} = \sum_{i=1}^N \left\{ \frac{(-i\hbar\nabla_i - \frac{e}{c}\mathbf{A})^2}{2m^*} + V_{\text{ext}}(\mathbf{r}_i) \right\} + \sum_{i<j}^N \frac{e^2}{\epsilon|\mathbf{r}_i - \mathbf{r}_j|} + g^*\mu_B B S_z, \quad (1)$$

where we have used the effective-mass approximation to describe electrons moving in the xy plane, surrounded by a background material of, e.g., GaAs with the effective electron mass $m^* = 0.067m_e$ and dielectric constant $\epsilon = 12.7$. The magnetic field \mathbf{B} is included using the symmetric gauge $\mathbf{A} = -B(y\mathbf{u}_x - x\mathbf{u}_y)/2$. In addition to the Zeeman coupling to the electron spin (last term above, GaAs value of g^* is around -0.44), the magnetic field introduces two new terms to the Hamiltonian, namely a “squeeze” term which is

$$\frac{e^2 B^2}{8m^* c^2} \sum_{i=1}^N (x_i^2 + y_i^2) = \frac{1}{2} m^* \left(\frac{\omega_c}{2} \right)^2 \sum_{i=1}^N r_i^2, \quad (2)$$

where $\omega_c = \frac{eB}{m^*c}$ is the cyclotron frequency. The second one is a “rotation” term:

$$\sum_{i=1}^N \frac{e}{2m^*c} \mathbf{B} \cdot \mathbf{r}_i \times \frac{\hbar}{i} \nabla = \frac{\omega_c}{2} L_z, \quad (3)$$

where L_z is the total angular momentum operator (z -component). These terms are always present, for all shapes of QDs. For this reason, in all the

Variational Monte Carlo for Interacting Electrons in Quantum Dots

cases where a finite B is present, there is a new harmonic term induced in the potential. The rotation term is a simple one for the cases that have rotational symmetry, as then the angular momentum is a good quantum number. For systems with lower symmetry, one needs to calculate the expectation value of the angular momentum operator. One can see that the rotation term lowers the energy of states that are rotating (on average) in the correct direction. This thus breaks the time-reversal symmetry and induces currents in the system.

We mainly present results for the case of the parabolic confinement, namely the one with an external potential

$$V_{\text{ext}}(\mathbf{r}) = \frac{1}{2}m^*\omega_0^2 r^2, \quad (4)$$

where ω_0 gives the strength of the confinement potential. One should note that it is possible to combine the external potential and the magnetic confinement as they are both parabolic. The simplest way to do this is to define a new confinement strength ω by $\omega^2 = \omega_0^2 + \omega_c^2/4$.

There are two obvious choices for the units to be used. The first one corresponds to the atomic units, but due to the effective mass and the dielectric constant, they are called the scaled atomic units. These are obtained by setting $\hbar = m^* = e = \epsilon = 1$. The second set of units commonly used is the ones of a harmonic oscillator. This is mainly applicable to the cases where the confinement potential is parabolic. A natural unit for the energy is given by the confinement strength $\hbar\omega$, and for the length, the simplest choice is to measure it in units of $l = \sqrt{\frac{\hbar}{m^*\omega}}$. The Hamiltonian in harmonic oscillator units can be written as

$$\mathcal{H} = \sum_{i=1}^N \left(-\frac{1}{2}\nabla_i^2 + \frac{1}{2}r_i^2 \right) - \frac{\omega_c}{2\omega}L_z + \frac{g^*\mu_B B}{\hbar\omega}S_z + \sum_{i<j} \frac{C}{r_{ij}}, \quad (5)$$

where C is the Coulomb strength ($C = \sqrt{\text{Ha}/\hbar\omega}\sqrt{m^*/m_0}/\epsilon = \sqrt{\text{Ha}^*/\hbar\omega}$, where Ha is the Hartree ≈ 27.2 eV, and Ha^* is the unit of energy in the scaled atomic units).

2.2. Single-particle States

The one-body problem for a parabolic QD is easily solved for an arbitrary magnetic field⁴. The single-particle wave functions (in harmonic-oscillator units and without the normalization which is irrelevant in VMC) are

$$\psi_{n,\pm|l|} \propto (x \pm iy)^{|l|} L_n^{|l|}(r^2) \exp[-r^2/2], \quad (6)$$

A. Harju

where l is the angular momentum quantum number, n is the shell index and $n' = (n - |l|)/2$, and L is the associated Laguerre polynomial. The two first polynomials L are

$$L_0^l(x) = 1 \quad (7)$$

$$L_1^l(x) = -x + l + 1, \quad (8)$$

and any L can be calculated from L_0^l and L_1^l using the recurrence relation

$$(n+1)L_{n+1}^l(x) = (2n+l+1-x)L_n^l(x) - (n+l)L_{n-1}^l(x). \quad (9)$$

The energy of a state with quantum numbers (n, l) is given by

$$E_{n,l} = (n+1) - \frac{\omega_c}{2\omega} l. \quad (10)$$

This is plotted in Fig. 1(a). One can compare this with lower-symmetry QDs, shown in Fig. 1(b)⁵. These four have a hard-wall potential of the

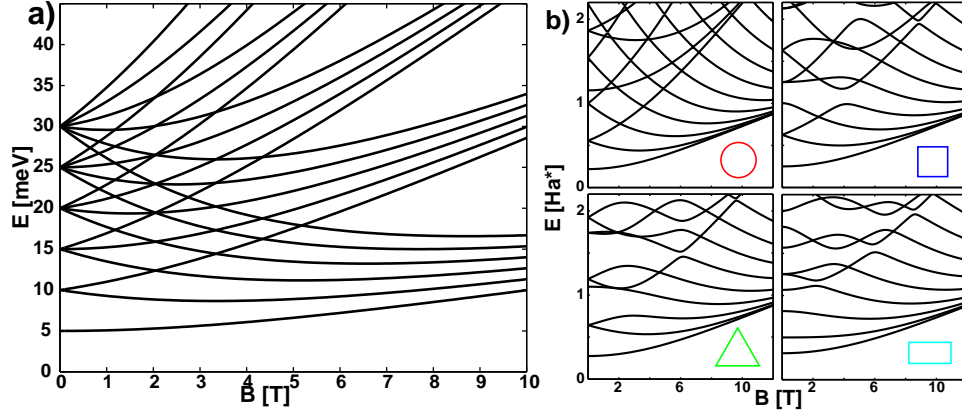


Fig. 1. (a) Total energy as a function of the magnetic field. GaAs parameter for the effective mass, i.e., $m^*/m_0 = 0.067$, $\hbar\omega_0 = 5.0$ meV. (b) Same for various hard-wall QDs, see Ref. 5 for more details.

shape shown in insets. One can see that the parabolic potential has the highest symmetry of the spectra shown, with high degeneracy in the $B = 0$ limit as well as a regular set of level-crossings at finite B values. The lowered symmetry affects the spectra at $B = 0$, and the lower the symmetry is, the more one sees anti-crossings of levels (instead of crossings).

In all the spectra of Fig. 1, one can see that the lowest states at strong B are bunched together to what corresponds to the lowest Landau level (LLL). For a parabolic QD, the LLL functions are of a very simple form, namely

$$\psi_l(\mathbf{r}) \propto z^l \exp\left[-r^2/2\right], \quad (11)$$

Variational Monte Carlo for Interacting Electrons in Quantum Dots

where $z = x + iy$, and only the angular momentum quantum number l is needed to label these states.

2.3. Non-interacting States

The non-interacting many-body states can be written as Slater determinants formed from the single-particle states of Eq. (6). As the single-particle states cross as a function of B , the non-interacting ground-state Slater determinants also have changes in the occupations. A general trend in the changes is that as B gets stronger, the occupations are mainly on the LLL. In the strong- B limit, all electrons occupy a state from the LLL. If we neglect the Zeeman-coupling to spin, the system has, for an even number of particles N , equal number of up- and down-spin electrons $N_\uparrow = N_\downarrow = N/2$. The non-interacting up-spin electrons occupy the N_\uparrow lowest states, and these have quantum numbers $l = 0, \dots, N_\uparrow - 1$, and the down-spin electrons have similar occupations. This non-interacting state corresponds to the filling factor $\nu = 2$ integral quantum Hall effect (IQHE) state. The correspondence to the IQHE state is, of course, only a qualitative one, as IQHE corresponds more to the thermodynamic limit. The reason why we now have $\nu = 2$ can simply be seen from the fact that the LLL states are doubly occupied (by both spin types). The up- and down-spin determinants can be written in a simple fashion, as they correspond to the Vandermonde determinants. Thus the unnormalized wave function has the form

$$\Psi(\mathbf{r}_1, \mathbf{r}_2, \dots, \mathbf{r}_N) = \exp \left[- \sum_{i=1}^N r_i^2 / 2 \right] \prod_{i_\uparrow < j_\uparrow}^{N_\uparrow} z_{ij} \prod_{i_\downarrow < j_\downarrow}^{N_\downarrow} z_{ij}, \quad (12)$$

where $z_{ij} = z_i - z_j$, and the spin indices are dropped for simplicity.

If all electrons are of the same spin type, one has a state with wave function

$$\Psi(\mathbf{r}_1, \mathbf{r}_2, \dots, \mathbf{r}_N) = \exp \left[- \sum_{i=1}^N r_i^2 / 2 \right] \prod_{i < j}^N z_{ij}, \quad (13)$$

which now corresponds to $\nu = 1$, as each LLL state is occupied by one electron. This state is called the *maximum-density droplet* (MDD), for the reason that it has the maximum density possible in the LLL⁶.

For a more general state, Eq. (9) can be used to simplify the determinant. To see this, consider states that have the same angular momentum l , but different shell index n . One can see in Eq. (9) that the state with shell index $n + 1$ can be obtained in a simple fashion from the states with the same l but that have shell indices n and $n - 1$. The basic determinant

A. Harju

calculation rule tells that one can remove from a row (or column) a linear combination of the other rows (or columns). Now in a Slater determinant, this simplification can be used to simplify Eq. (9) for the states that have all states with the same l but lower n occupied. This simplified recurrence reads

$$\tilde{L}_{n'+1}^l(r^2) = r^2 \tilde{L}_{n'}^l(r^2) , \quad (14)$$

where we have also dropped the normalization and used that in QDs, we have $x = r^2$. Noting that $L_0^l(x) = 1$, one finally gets

$$\tilde{L}_{n'}^l(r^2) = r^{n-|l|} . \quad (15)$$

The configurations that have all states with same l but lower n occupied are called n -compact. For these configurations, one can use for the one-body states the simplified form

$$\psi_{n,\pm|l|} \propto (x \pm iy)^{|l|} r^{n-|l|} \exp[-r^2/2] . \quad (16)$$

One should note that all the lowest-energy states of a non-interacting N -electron QD are n -compact. In addition, there is no obvious reason why interactions would favor non- n -compact states.

2.4. Separation of the Center-of-Mass Motion

For a parabolic QD, the Hamiltonian of Eq. (5) has an important simplifying property; the center-of-mass (CM) and the relative motion of electrons decouple. To see this, one has to make use of the identity

$$\sum_{i=1}^N r_i^2 = N r_{\text{cm}}^2 + \frac{1}{N} \sum_{i < j}^N r_{ij}^2 , \quad (17)$$

where \mathbf{r}_{cm} is the coordinate for the CM.

The separation of the CM and relative motion has an interesting consequence, namely that if the wave function for the non-interacting state is an eigenstate of the CM motion, then turning on the electron-electron interaction can change only the relative motion part of the wave function. This means that the many-body wave function can be written as a product of the CM and relative wave functions as

$$\Psi = \Psi_{\text{cm}}(\mathbf{r}_{\text{cm}}) \Phi(\{\mathbf{r}_{ij}\}_{i < j}) , \quad (18)$$

where the Φ -part contains all non-trivial effects of interactions, and the CM-part is a solution for a harmonic oscillator, see, e.g., Ref. 7 for more details.

Variational Monte Carlo for Interacting Electrons in Quantum Dots

To see how this affects the topology of the wave function, one should note that the exponential factor is the same in all states of Eq. (6), and it can be taken out from any determinant made of these as

$$\exp \left[-\frac{1}{2} \sum_{i=1}^N r_i^2 \right] = \exp \left[-\frac{1}{2} N r_{\text{cm}}^2 \right] \exp \left[-\frac{1}{2N} \sum_{i<j}^N r_{ij}^2 \right]. \quad (19)$$

Now if one would like to include a variational parameter α to the exponential as $\exp[-\alpha r_i^2/2]$, one would directly see from the argument above that the optimal value for α should be one. Other choices would raise the energy because the CM-part would not be exact. In addition, even if varying α would lower the interaction energy, this kind of effect should be directly put in to the wave function of relative coordinates, for example using two-body correlation factors. For this reason there is no similar screening of the external potential as in the case of atoms. If one, however, would apply a Hartree-Fock approach for the problem, one certainly lowers the energy by adjusting the single-particle states. This is because one cannot change the relative-motion part of the Hartree-Fock wave function as it is, by definition, only a single Slater determinant.

We can thus have the following important conclusion: If the relative motion part of the many-body wave function is treated in a reasonable accuracy, the single-particle states in the determinant part of the Slater-Jastrow wave function (see Section 2.5.) can be taken to be the non-interacting ones. In many VMC studies, one uses single-particle states from a mean-field theory in the construction of the Slater determinants. This is not, however, the most accurate strategy, based on the arguments presented above⁸.

The separation has also a second effect, namely that the far-infrared absorption spectra of parabolic QDs are trivial, and do not depend on electron number or the interaction between electrons. For lower symmetries of the confinement potential, interesting spectra are obtained^{9,10}.

2.5. Wave Functions for Quantum Dots

The most commonly used VMC wave function is the Slater-Jastrow one of the type:

$$\Psi = D_{\uparrow} D_{\downarrow} \prod_{i<j}^N J(r_{ij}), \quad (20)$$

where the two first factors are Slater determinants for the two spin types, and J is a Jastrow two-body correlation factor. We neglect here the three-body and higher correlations. This form of a wave function has shown to be very accurate in many cases².

A. Harju

One can easily generalize the Jastrow part to also contain higher-order correlations. This might not be very important in the present case, as we are studying a two-dimensional system. Basically, by lowering the dimensionality of the problem, one enhances the correlation effects, because particles have less degrees of freedom to avoid each other. On the other hand, the lowered dimensionality makes it more difficult for more than two particles to get close to each other, and in this way the relative importance of the correlations beyond the two-particle level gets smaller as the dimensionality is lowered¹¹.

For the two-body Jastrow factor we use here a simple form of

$$J(r) = \exp\left(\frac{Cr}{a + br}\right), \quad (21)$$

where a is fixed by the cusp condition to be 3 for a pair of equal spins and 1 for opposite ones, and b is a parameter, different for both spin-pair possibilities. C is the scaled Coulomb strength. For a d dimensional Coulombic system, the cusp condition can actually be found to be

$$\frac{J'(r)}{J(r)} = \frac{C}{d - 1 + 2l}, \quad (22)$$

where l is the relative angular momentum between particles. The actual value of l depends on the wave function form, but for electrons with opposite spins $l \geq 0$ and for parallel spins $l \geq 1$.

In the simplest form of the determinant in Eq. (20), the single-particle wave functions depend only on the coordinates of one electron. However, in some complicated cases the single-particle states must depend on all particles. This can be the case for some QD states, too. If one would recast this type of determinant to a basic one with simple single-particle states, more than one determinant is needed.

The basic reason why the Slater-Jastrow wave function is accurate in many quantum systems is that there is one most important configuration in an exact expansion of the wave function in terms of configurations. In addition, the next configuration (of the same symmetry) is in the successful cases clearly higher in energy. One can then view the addition of the Jastrow factor as a minor correction to a single-determinantal wave function.

This reasoning might, however, be too trivial for QD's. As shown in Section 3.1. for the case of two electrons, the Slater-Jastrow form of Eq. (20) is actually exact for any interaction strength. This means that even in the limit $C \rightarrow \infty$ where the overlap of a single determinant wave function with the exact one goes to zero, the Slater-Jastrow combination is exact. A similar finding can be seen in a six-electron QD at $C \rightarrow \infty$, see Section 3.2. below.

Variational Monte Carlo for Interacting Electrons in Quantum Dots

The arguments given above work reasonably well from the zero magnetic field case up to rather strong magnetic fields. However, when the magnetic field is so strong that the system is in a fractional quantum Hall effect regime, things change dramatically. The interesting and rich physics of this regime is namely given by the fact that there is a high degeneracy of single-particle states in the lowest Landau level. There are cases when the wave function in this regime can be written as a Slater-Jastrow one, and the Laughlin states are interesting examples of this¹². But there are also cases when such a simplification might not work well.

2.6. Variational Monte Carlo

A brief review of the variational Monte Carlo (VMC) method can be found in Ref. 2. In our implementations, we typically perform VMC with around ten walkers at the same time. There are two basic reasons for this, namely that as these walkers are independent, we can do a rigorous error estimate over them. In addition, these are needed for the wave function optimization presented below.

If our N_W walkers have estimates $\{a_i\}_{i=1}^{N_W}$ for an observable O , the best estimate for O is the mean of a_i 's. The error estimate can be obtained from the law of large numbers, and it states that we can approximate the error in our estimate as the standard deviation of the set $\{a_i\}_{i=1}^{N_W}$ divided by the square root of N_W . If one would have only one walker, one should perform by some means an analysis of the autocorrelation length for the observable in question to get a rigorous error estimate.

Lin *et al.*¹³ have shown that in the case of real wave functions and energy minimization, the derivative of the energy E with respect to a variational parameter α_i is simply

$$\begin{aligned} \frac{\partial E}{\partial \alpha_i} &= \frac{\partial}{\partial \alpha_i} \frac{\int \Psi \mathcal{H} \Psi}{\int \Psi^2} \\ &= \frac{\int \Psi' \mathcal{H} \Psi}{\int \Psi^2} + \frac{\int \Psi \mathcal{H} \Psi'}{\int \Psi^2} - 2 \frac{\int \Psi \mathcal{H} \Psi}{\int \Psi^2} \frac{\int \Psi' \Psi}{\int \Psi^2} \\ &= 2 \left\langle E_L \frac{\Psi'}{\Psi} \right\rangle - 2 \langle E_L \rangle \left\langle \frac{\Psi'}{\Psi} \right\rangle, \end{aligned} \quad (23)$$

where $\Psi' = \partial \Psi / \partial \alpha_i$, $E_L = \frac{\mathcal{H} \Psi}{\Psi}$ is the local energy and the average $\langle \dots \rangle$ is over a set of configurations generated with, e.g., the Metropolis algorithm¹³.

Some possibilities for optimizing the parameters are presented in Ref. 2. These do not benefit from the simple formula for the gradient of the parameters given above. Especially for this reason, we think that the optimization

A. Harju

can be done in a more efficient fashion than is explained in Ref. 2. One possibility for this is the stochastic gradient approximation (SGA) method¹⁴, which is an optimization method tailored for functions with statistical uncertainty. The SGA algorithm in the original formulation did not use the simple gradient formula.

Given a set of N_W walkers, one can calculate an approximation for the gradient of the optimized parameters with respect to the cost function by Eq. (23). To minimize the cost function, one should move in the direction of the negative gradient. Unfortunately, the step length needed is not trivial to estimate. In SGA, the step is adjusted dynamically by a parameter γ . So at the i 'th optimization step, the parameters are changed by

$$\alpha_{i+1} = \alpha_i - \gamma_i \nabla \alpha F_C, \quad (24)$$

where F_C is the cost function. The step length γ_i is changed in such a fashion that it monitors the changes in sign of the gradient. There is a simple reason for this: if the sign of the gradient remains the same over the steps, one is approaching the minimum of the cost function and there is no reason to slow down (actually, one could increase the step length). If the sign of the gradient oscillates, one most probably makes too long steps in the optimization and the minimum is somewhere close by and the optimization jumps each time over it to the other side of the minimum. Thus it would be better to make γ smaller. Of course, our gradient can change sign simply due to the statistical noise in the gradient. In actual codes, each parameter has an integer counter that counts the times the sign of the gradient has changed. The value of this integer j at step i then defines the value for $\gamma_i = \gamma_0 j^{-0.6}$, where γ_0 is an adjustable parameter to give an overall length scale for the optimization steps. The choice of power -0.6 is not arbitrary, see Ref. 14 for limits for it. In actual calculations, one can start with a small value of γ_0 and make it larger every time the gradient keeps a same sign. This can also be done in an efficient fashion by generalizing the integers j to a real numbers that start from one but then are, e.g., halved at each step where the sign of the gradient does not change. After a first change of sign is obtained, one can then switch to damping (like $j = j + 1$) as one has then reached the surrounding of the minimum being searched.

To show the performance of the SGA scheme in actual simulations, a six-electron MDD case is studied. The wave function is thus a product of the wave function of Eq. (13) multiplied by a product of Jastrow factors in Eq. (21). We have set $C = 1$, and the results are reported in units of the harmonic oscillator. In this case, we only need to optimize one parameter, the b in Jastrow of Eq. (21). First, we have performed 60 short simulations of 10 seconds each for b values between 0.7 and 1.3. The resulting energies

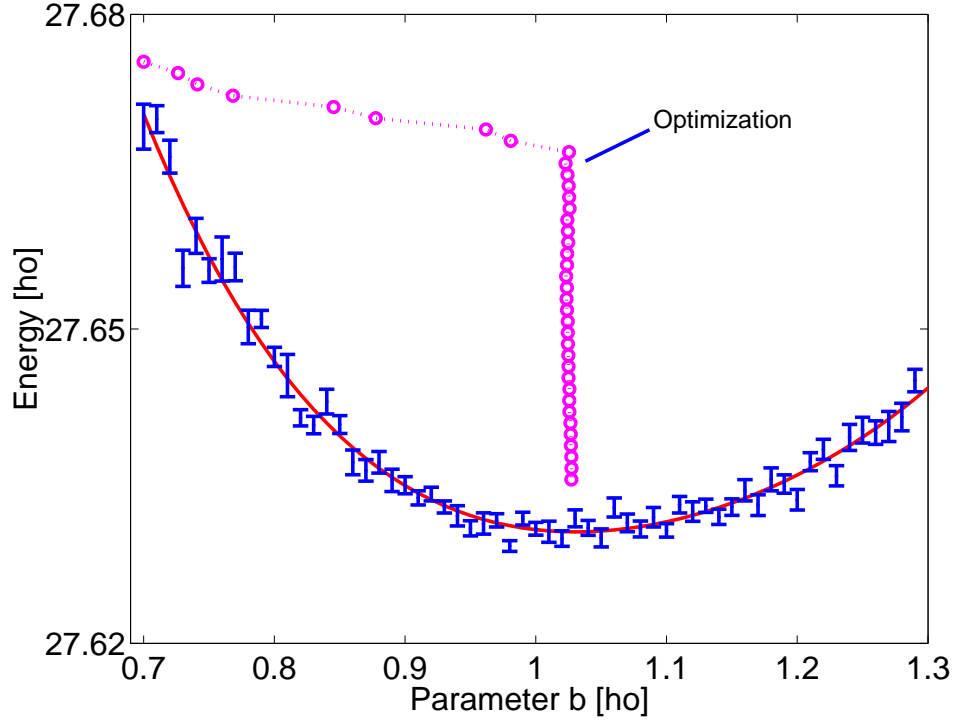


Fig. 2. Total energy as a function of the Jastrow parameter b . Solid line is a polynomial fit to energies, shown to guide the eye. Circles present the SGA parameter optimization path. Each energy value is from a 10 second run, and all the optimization steps shown take 0.1 seconds.

and the error estimates are shown in Fig. 2. One can see that the energy has a minimum value around $b \approx 1$, the actual position being unclear due to the statistical noise. In Fig. 2 we also plot the parameter values obtained by the SGA optimization that has started from $b = 0.7$ and ends around $b \approx 1.03$. We have used $N_W = 10$ walkers in optimization. One can see that it takes less than ten steps to reach the optimum value. It is clear from these numbers that the optimization is very fast. The time needed for all the optimization steps shown is only 1/100 of each of the independent simulations done, that is, only 0.1 seconds.

One reason why the optimization is so fast can be seen in Fig. 3, where the derivative of the energy is plotted. One can namely see that the statistical noise in the gradient is much smaller than in the energy. The data of Fig. 3 also shows that the parameter value of $b \approx 1.03$, found by the SGA algorithm, is a very accurate one. In addition to having smaller fluctuation than energy,

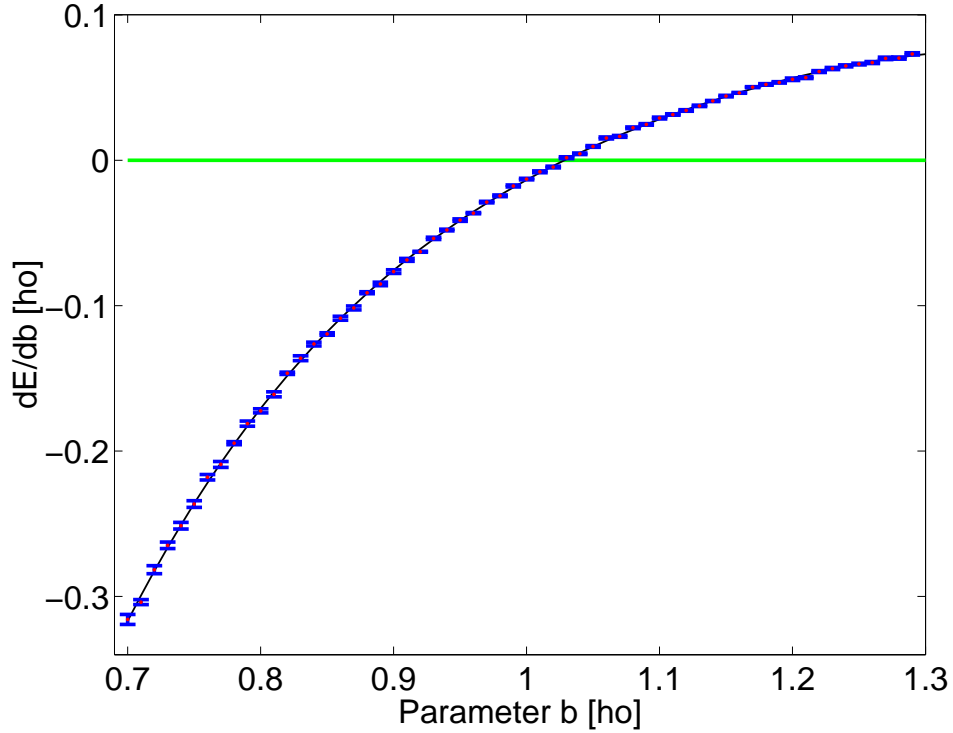


Fig. 3. Derivative of the total energy with respect to Jastrow parameter b as a function of b . Each derivative from a 10 second run like in Fig. 2. It is interesting to note that the gradient has much smaller fluctuation than the energy.

also the underlying statistical distribution of the analytic gradient is in many cases very good for the optimization. In Fig. 4, the histogram of the gradient values is shown for the case of $b = 0.7$ for a set of around 4000 evaluations of the gradient. An interesting feature is that all the gradient values in this set have the same sign. This is very good for the SGA scheme where the actual absolute value of the gradient is less important than the sign of the gradient. One should note that closer to the minimum, the gradient distribution of the present case changes to a rather symmetric one.

One can actually show that in a case of a one-dimensional harmonic oscillator, defined by the Hamiltonian

$$\mathcal{H} = -\frac{1}{2} \frac{d^2}{dx^2} + \frac{1}{2} x^2, \quad (25)$$

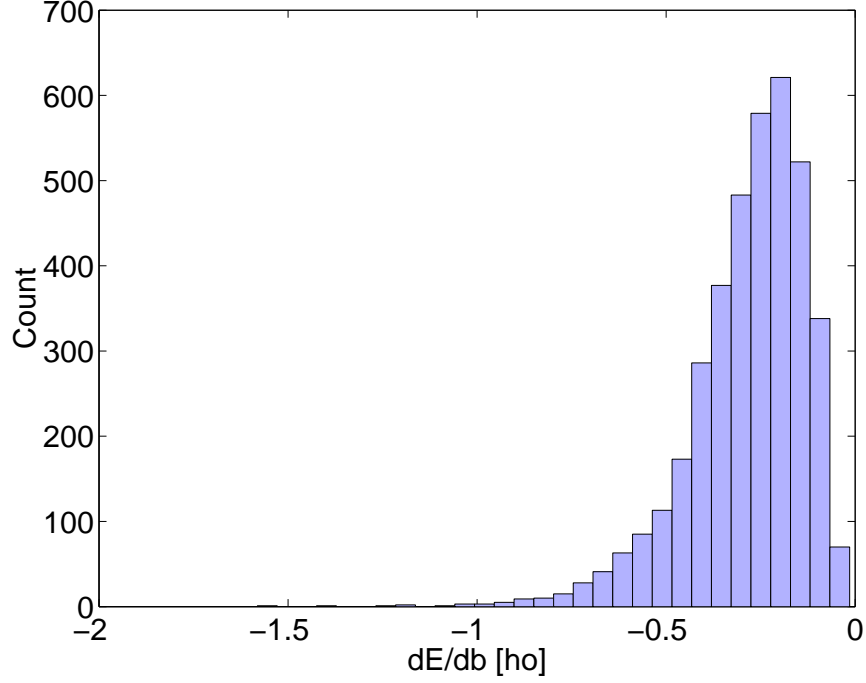


Fig. 4. The histogram of the gradient values for the case of $b = 0.7$. All the gradient values have the same sign.

and using a variational wave function of

$$\psi(x) = \exp(-\alpha x^2) , \quad (26)$$

the analytic gradient formula gives a rather interesting optimization problem where the distribution of the gradient is such that no matter how small sample one has in Eq. (23), the sign of the energy gradient is always correct. The gradient is found to be

$$\frac{dE}{d\alpha} = \left(1 - \frac{1}{4\alpha^2}\right) \sigma^2 , \quad (27)$$

where σ^2 is a variance of a function over points sampled from ψ^2 , and thus positive. One thus ends up with a stochastic optimization problem where the value of the optimized function and its derivative with respect to parameter is known only with a statistically limited accuracy, but the sign of the gradient has *not* statistical noise and can be found exactly by very limited statistics. Interestingly, similar optimization problem is found for the Hydrogen atom with wave function $\psi(r) = \exp(-\alpha r)$. It might be that the special form of

A. Harju

the optimization problem is related to the underlying Gaussian and Poisson distributions and their width which is proportional to optimized parameter.

3. RESULTS

The results are split into three parts, those for zero magnetic field, moderate magnetic field, and high magnetic field. The splitting is, of course, not unique, but we feel it is justifiable. By a moderate magnetic field we mean magnetic field values where the system, in the thermodynamic limit, would be in an IQHE state. The strong magnetic field then corresponds to a fractional quantum Hall effect (FQHE) regime. The logic behind this division is that the physics in these regimes is rather different. For example, the physics of IQHE can still be described, in a reasonable fashion, by arguments on a single-particle level. However, when the system is in the FQHE regime, the electron-electron interaction dominates and all single-particle levels are nearly degenerate. This difference is then reflected in the nature of the many-body wave functions: In the IQHE regime, a single configuration is in most cases adequate, but for FQHE-states several configurations are needed. One would expect that the mean-field theories are still reasonably accurate in the IQHE regime, but for the FQHE cases, a real many-body theory is needed. The reason for splitting the zero magnetic field from the moderate one is that even a small but finite magnetic field changes the physics in an important fashion. For example, the time-reversal symmetry is broken as soon as finite magnetic field is included. On the other hand, the transitions in finite quantum systems are in general either smooth or of the level-crossing-type. For this reason the split introduced here might not always be clear-cut. Before presenting real many-body results, the results of the simplest non-trivial case, namely the two-electron one, are presented. As will be shown below, it allows one to understand many properties of the results for larger particle numbers.

3.1. Two Electrons

The problem of two electrons in a parabolic confinement, subject to external magnetic field, is in principle four-dimensional. However, after separating the center-of-mass and relative motion and using the rotational symmetry, the problem is reduced to a one-dimensional one.

As a special case, the one where the relative interaction strength $C = 1$

Variational Monte Carlo for Interacting Electrons in Quantum Dots

in Eq. (5) and $B = 0$, the (unnormalized) solution can be written as

$$\Psi(\mathbf{r}_1, \mathbf{r}_2) = (1 + r_{12}) \exp[-(r_1^2 + r_2^2)/2] , \quad (28)$$

with energy $E = 3$.

This state has a simple generalization for finite B and any interaction strength, namely

$$\Psi(\mathbf{r}_1, \mathbf{r}_2) = z_{12}^m J(r_{12}) \exp \left[-(r_1^2 + r_2^2)/2 \right] , \quad (29)$$

where m is the relative angular momentum of the electrons. Varying the interaction strength only changes the J -part of the wave function. It turns out that a simple Jastrow factor of the type

$$J(r) = \exp \left[\frac{Cr}{(2|m| + 1)(1 + br)} \right] \quad (30)$$

is a rather accurate approximation for the true solution¹⁵.

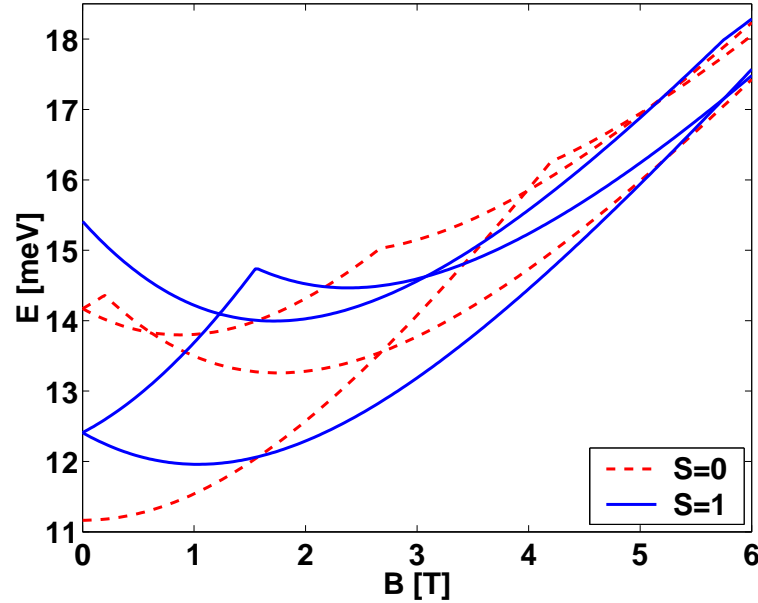


Fig. 5. Energy for a two-electron GaAs QD. Confinement strength is 3 meV. Two crossings in the ground state are seen.

In addition to changing the relative-coordinate function J above, the interaction has a second, even more interesting effect. Namely, when the

A. Harju

magnetic field is made stronger, the interaction favors a state that has a higher angular momentum than the $B = 0$ one with $m = 0$, see Fig. 5. The reason for this is that the electrons are moving further apart as m is made larger. The states with even m correspond to total spin $S = 0$, and the odd ones to $S = 1$. Now, without Zeeman term, the spin would oscillate between zero and one, but if the Zeeman interaction is included, it lowers the energy of the triplet state, and the strong B ground state is found to be $S = 1$.

One can analyze the phase structure of the wave function by fixing one electron and studying the phase as the other electron is moved^{16,17,18}. One can see from Eq. (29) that the phase of the wave function changes by $2\pi m$ as our probe electron circulates the fixed one. In addition, the conditional density is zero at this point. One can identify this zero as a vortex (with winding number m)¹⁶, which actually corresponds to m flux quanta on top of the fixed electron. In this way, the magnetic field is used to keep the two electrons further apart. See Fig. 6.

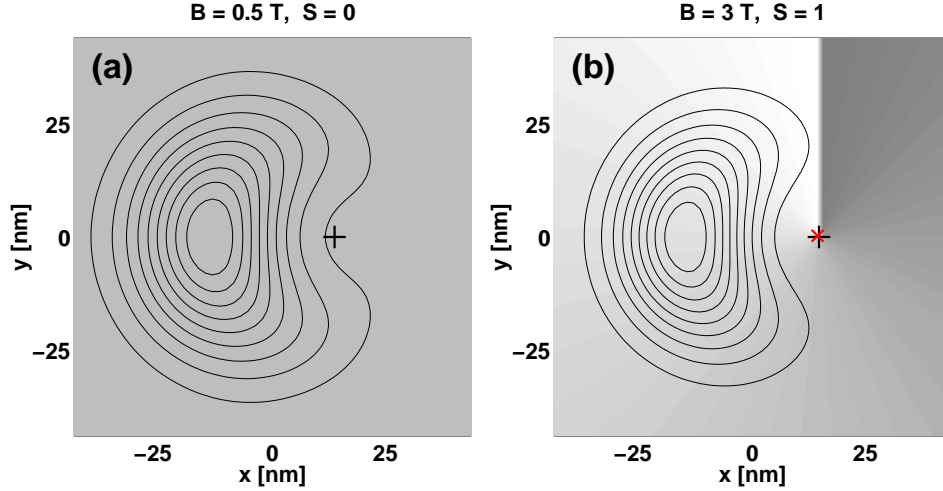


Fig. 6. Conditional density and phase for the two-electron QD of Fig. 5. One electron is fixed at “+”, and the conditional electron density is presented by contours and the phase by the gray-scale. The phase changes from π to $-\pi$ on the lines where shadowing changes from the darkest gray to white. (a) corresponds to the $S = 0$ state at a weak magnetic field, and (b) to the $S = 1$ state with one vortex, marked with “x”, on top of the fixed electron.

If one lowers the symmetry of the confinement potential, the wave function is not as simple anymore. However, some similarities can still be found in the phase structure of the wave function and in the behavior of the total spin¹⁹.

3.2. Zero Magnetic Field

The most interesting limit in zero magnetic field is the one where the confinement is extremely weak. In this limit, the interactions dominate in the energy, and the system approaches the classical limit²⁰. Before the classical limit, one sees *Wigner molecule* formation. In this regime, the electrons start to localize (in relative coordinates), so that if one fixes all but one of the electrons and studies the conditional density for the remaining one, the density is seen to get more and more peaked as the system approaches the classical limit²¹.

The energies obtained with a single-determinant-Jastrow wave function are extremely accurate in the Wigner-molecule limit²¹. The energies for spin polarized and unpolarized cases are shown in Fig. 7(a). For the six-electron QD, we found a spin polarization in the system before the Wigner-molecule limit, see Fig. 7(b). One should note that the exact diagonalization results are less accurate than the VMC ones, and the results obtained with a path-integral Monte Carlo have around two orders of magnitude larger statistical uncertainty and are higher in energy, see Ref. 21 for details. In finite systems

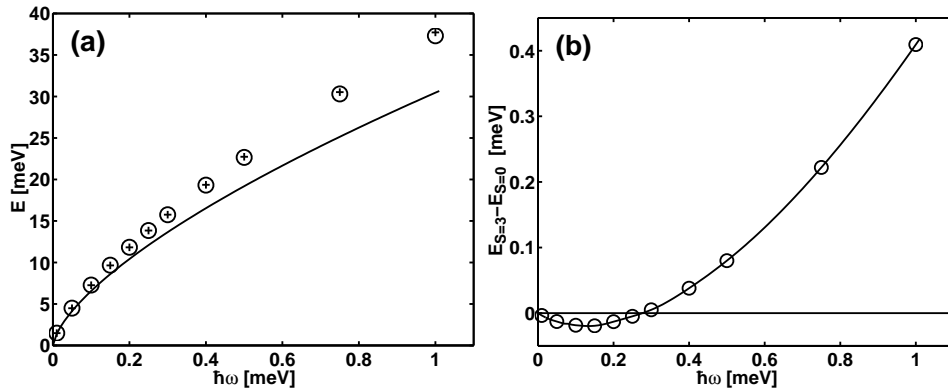


Fig. 7. (a) Total energy for spin states $S = 3$ (marked with pluses) and $S = 0$ (circles) as a function of $\hbar\omega$. The line presents the classical energy. (b) Energy difference between the spin states $S = 3$ and $S = 0$ as a function of $\hbar\omega$. The line is to guide the eye.

like this, the shell structure still plays a role. For this reason, a six-electron QD is a good candidate for more general conclusions, as both unpolarized and fully spin-polarized configurations correspond to closed shells. For open shells, the wave function might not always be as simple as for the closed-shell cases²¹.

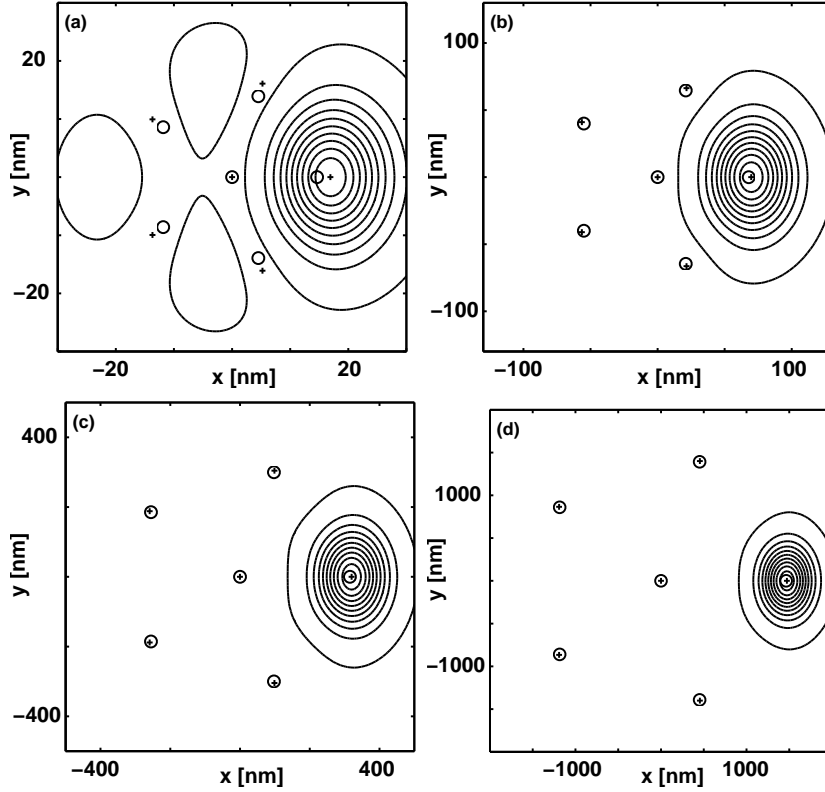


Fig. 8. Conditional probability density for the right-most electron. The contours are spaced uniformly from 0.01 to 0.91. We mark with a plus the most probable electron positions, and with a circle the classical positions. The confinement strength $\hbar\omega$ is: (a) 10 meV, (b) 1 meV, (c) 0.1 meV, and (d) 0.01 meV.

The most probable configuration \mathbf{R}^* , found by maximizing the density $|\Psi(\mathbf{R})|^2$, should approach in the limit of weak confinement the classical electron positions. This is not, however, enough to show that the system is close to a classical one. One can study the quantum fluctuations very conveniently using the conditional single-particle probability distribution $\tilde{\rho}(\mathbf{r})$, defined as

$$\tilde{\rho}(\mathbf{r}) = \left| \frac{\Psi(\mathbf{r}, \mathbf{r}_2^*, \dots, \mathbf{r}_N^*)}{\Psi(\mathbf{r}_1^*, \mathbf{r}_2^*, \dots, \mathbf{r}_N^*)} \right|^2, \quad (31)$$

where the coordinates \mathbf{r}_i^* are fixed to the ones from the most probable configuration \mathbf{R}^* . In the classical limit, the density $\tilde{\rho}(\mathbf{r})$ is more and more peaked around the classical position \mathbf{r}_1^* , but still shows quantum fluctuations. This

Variational Monte Carlo for Interacting Electrons in Quantum Dots

is shown in Fig. 8

The calculation of $\tilde{\rho}$ is very easy in VMC. One should first, of course, find the most probable electron positions. In doing this, the gradient of the wave function (also needed for the calculation of the local energy, and for this reason usually done analytically) is very useful. After that, one moves the “probe electron” to all points where the value of $\tilde{\rho}$ is wanted, and evaluates the ratio of wave functions as in Eq. (31). This ratio is automatically done while sampling the configurations in a VMC simulation. One should also notice that $\tilde{\rho}$ does not contain noise unlike many more common VMC observables, such as the density or the radial pair distribution function.

It is rather surprising that non-interacting single-particle states can be used for rectangular hard-wall QD’s also²². Our VMC results using these agree very well with the density-functional theory data^{22,23}. To see this, the addition energies $\Delta(N)$ (defined as a second difference in total energies $E[N+1] - 2E[N] + E[N-1]$) are plotted in Fig. 9. The differences between the results of the two different methods are extremely small in all cases. The data shows that by tuning the ratio of the two axis of the system, the shell structure of the electronic structure can be tuned in a controllable fashion. This is one of the aims in novel microelectronics, namely that one can engineer the properties of the nanoscale semiconductor system to suit the need at hand. This parameter-tuning is, of course, not possible in a simple way in the cases of atoms and molecules. The parameter-tuning also has an interesting effect on the theoretical calculations. One can study how various approximations perform as a function of the change in the system parameter. This is done in Fig. 10, where we compare the total energies from an exact diagonalization to a density-functional one for the case of a four-electron rectangular QD. The parameter we change is the side-length ratio β . The mean-field approach has a broken-symmetry solution, and our analysis shows that the energy lowering due to breaking the symmetry is too large, and in addition, the broken-symmetry solution results from the fact that the system naturally consists of two important configurations²³. It might be possible to treat several configurations by a mean-field approach, see Ref. 23 for a suggestion, but it is not trivial.

One should note that also in VMC, it is very difficult to know beforehand if one needs a multi-configuration wave function or not. Some analysis can be performed based on the single-particle energetics. However, even in cases where one can form several different configurations that are close in energy, it is not clear that all these configurations are relevant for the ground state. Of course, symmetry plays again role here. As a concrete example, one can compare the four-electron $S = 0$ states of a parabolic and a square hard-wall QD. The single-particle states of the parabolic case can be obtained

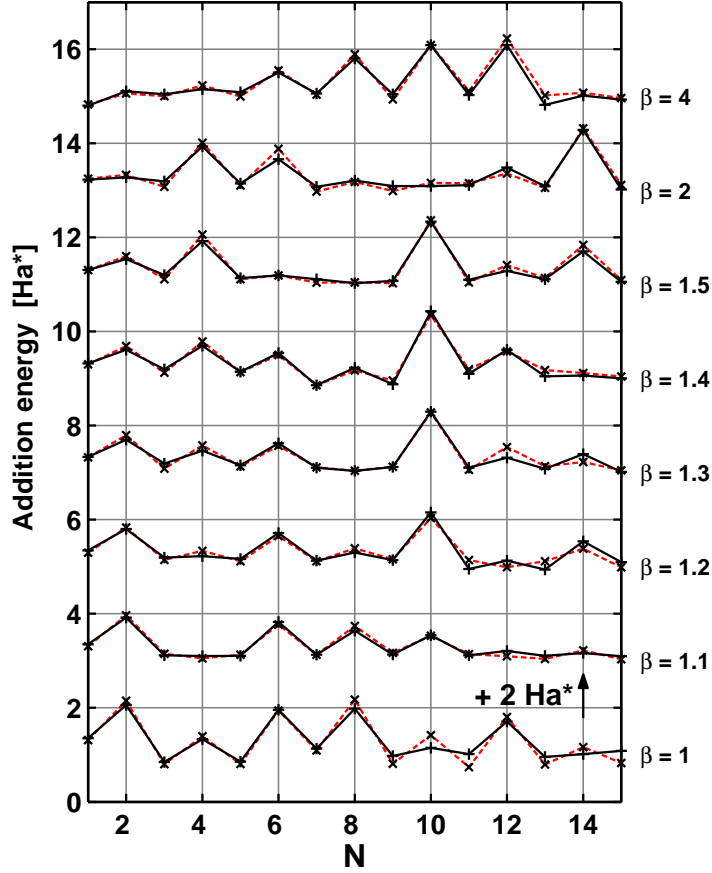


Fig. 9. Addition energy spectra for rectangular quantum dots with different axis ratio β . The density-functional theory and VMC results are given by pluses and crosses connected with solid and dashed lines, respectively.

from Eq. (16), and the ones for the square one in Fig. 11 with the relevant ground-state configurations. The relevant configurations for the parabolic case can be found in a similar fashion from the three lowest single-particle states (by replacing the (n_x, n_y) states by the lowest (n, l) ones). From the four configurations, one can form both $S = 1$ and $S = 0$ states with $S_z = 0$. The $S = 1$ state with $S_z = 0$ consists of the configurations C_3 and C_4 with equal weight. This is degenerate with the $S = S_z = 1$ state, which is a single determinant. This configuration can be obtained from C_3 or C_4 by flipping the down-spin from the higher state. One can, however, find a truly two-configuration $S = S_z = 0$ state from the configurations C_1 and C_2 . Without the electron-electron interaction, the states $\Psi_{\pm} = C_1 \pm C_2$ have the same

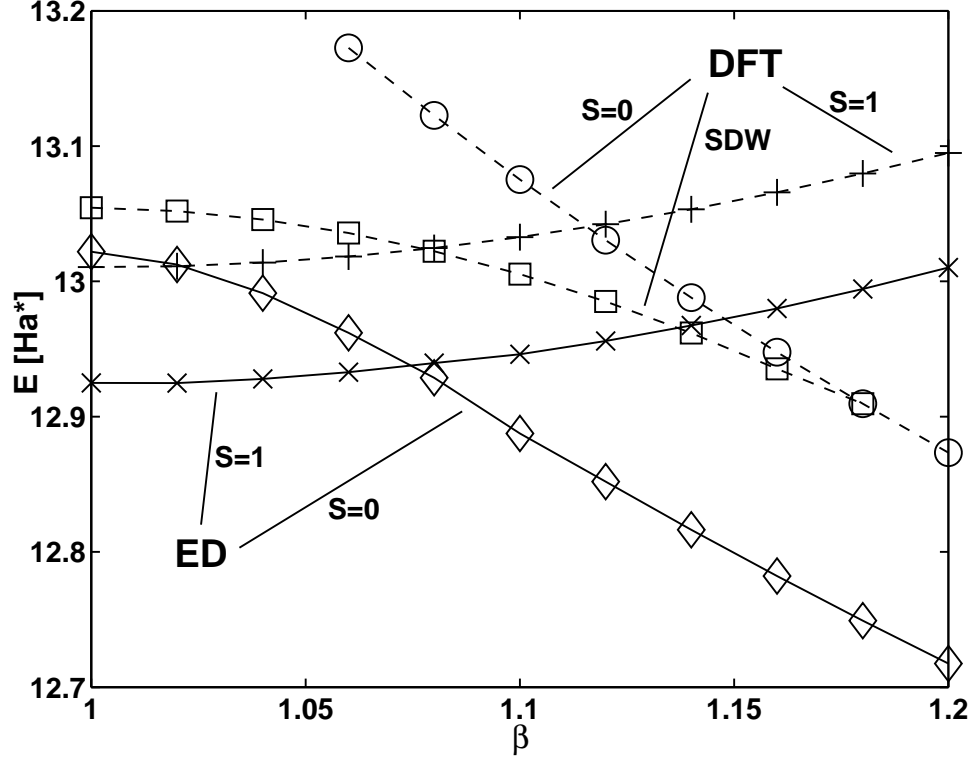


Fig. 10. Energy of the four-electron dot as a function of β . The solid lines present exact energies, we use crosses for $S = 1$ and diamonds for $S = 0$, correspondingly. The dashed lines are density-functional theory energies, pluses for $S = 1$, boxes for the $S = 0$ broken-symmetry solution, and circles for the symmetric $S = 0$ energy.

energy. However, when the interaction is present, the degeneracy of these states is split, and one of them is lowered in energy. This can directly be seen from the Hamiltonian matrix on the basis of these two configurations

$$H = \begin{pmatrix} E_1 & \delta \\ \delta & E_2 \end{pmatrix}, \quad (32)$$

where the energies E_i are for configurations C_i and δ denotes the coupling of the configurations. If one performs the same analysis for the two configurations of the parabolic case, one actually finds that the coupling between the two configurations is zero ($\delta = 0$). This means that the configurations do not mix. The reason for this is symmetry. One can find this out by calculating the Coulomb matrix element between the configurations, but it is also

A. Harju

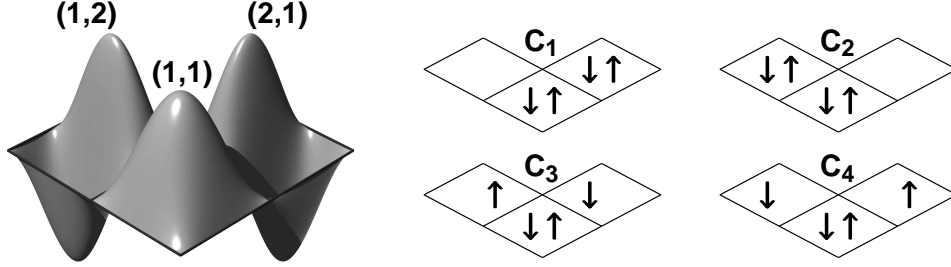


Fig. 11. Left panel: The three lowest single-particle states and their quantum numbers (n_x, n_y) . The (1,1) state is a positive sine function and both of the two higher states have one node (on x and y axis, correspondingly). Right: Electron occupations for the four important $S_z = 0$ configurations C_i .

possible to see this directly from symmetry. The two configurations in the parabolic case correspond to ground states with angular momentum ± 2 . As the problem has circular symmetry, the angular momentum is a good quantum number both for the single- and many-particle states. In this way the configurations with different symmetry do not mix. One should note that here we have used real wave functions for the square QD and complex for the parabolic one. If one would use real ones for the parabolic case, several configurations are needed⁸. However, the use of complex wave functions in a square case does not bring the wave function to a single-configuration one.

3.3. Integral Quantum Hall Effect Regime

The finite B lowers the symmetry of the parabolic QD, as the states that form shells at $B = 0$ are not degenerate anymore. This can be seen in Fig. 1. The reason for this is the “rotation” term in the Hamiltonian, discussed in Section 2.1., that lowers the energy of states that rotate to the correct direction, and highers the ones with an angular momentum of opposite sign.

A single-determinant-Jastrow wave function is still accurate in the IQHE regime²⁴. One can also find good agreement with the experimental transition points²⁴. This can be seen in Fig. 12, where the curve shows the measured data, with kinks at the transition points, and the markers shows the B -values where the VMC finds a change in the ground state configuration. The VMC parameters used are $m^*/m_0 = 0.067$, $\epsilon = 12.9$, $\hbar\omega_0 = 4.5$ meV, $g^* = -0.44$, and $V_{ee} = \alpha \frac{e^2}{\epsilon r_{ij}}$ with $\alpha = 0.7$. Basically, we have two parameters to tune, but we have tried to extract them from the experimental data. The con-

Variational Monte Carlo for Interacting Electrons in Quantum Dots

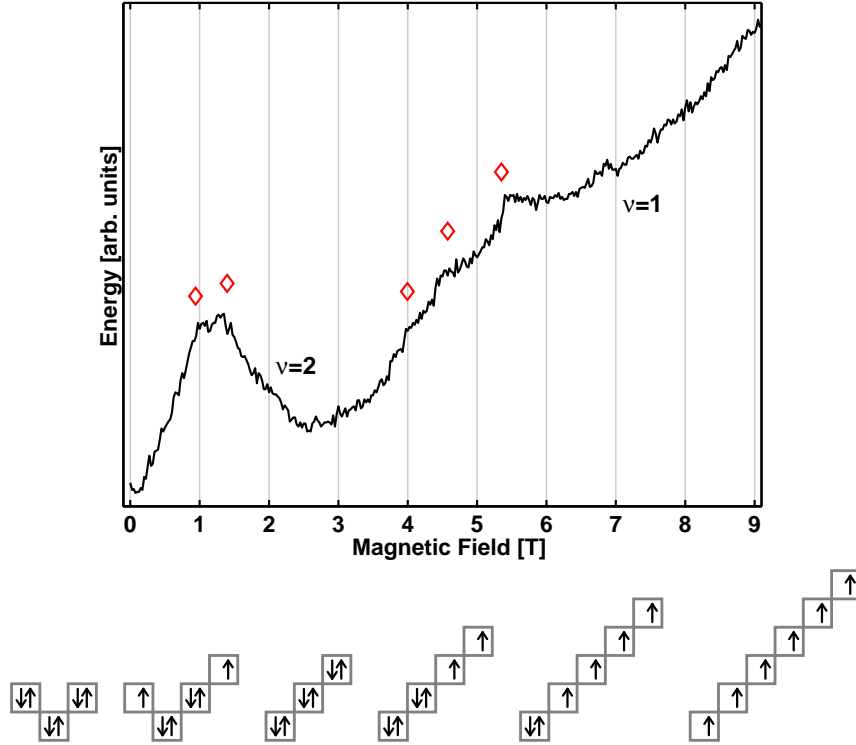


Fig. 12. Upper panel: Experimental energy as a function of the magnetic field B for $N = 6$ QD. The kinks show the transition points where the lowest energy state changes. The B -values of the VMC transition points are marked with ' \diamond ' (vertical positions arbitrary). The two ground-state regions that are related to quantum Hall states with filling factors $\nu = 1$ and 2 are shown. Lower panel: Electron occupations of the lowest energy states.

finement value used is a reasonable one compared with the experimental value of $\hbar\omega_0 \approx 5$ meV for the one-electron dot, as the confinement is weaker for larger electron numbers. The scaling of the Coulomb interaction value $\alpha = 0.7$ is obtained from the experimental transition point for the $N = 2$ case, assuming that the confinement strength is nearly the same as for one-electron QD. The choice of α means that the electron-electron interaction is only 70 percent of what one would assume from the material parameters. There are two effects that cause this. The first is the softening of the interaction at small electron-electron distances. This is due to the fact that in our model we completely neglect the third spatial dimension. In a realistic case, when the electrons approach each other, they can use this dimensionality to

A. Harju

avoid each other. This results in an interaction potential that is effectively softer at small electron-electron distances. One possibility to insert this in to theory would be to use an interaction of the type

$$V(r_{ij}) = \frac{C}{\sqrt{\delta^2 + r_{ij}^2}}, \quad (33)$$

where δ is directly proportional to the finite width of the system. The second effect is that in experimental setups, the surrounding metallic gates can screen the electron-electron interaction at large inter-electron distances. One can use different approximations for the screening, but qualitatively, the effect of this is also that the interaction becomes weaker. We have, in some approximation, taken these into account by tuning the interaction by the parameter α . What makes this approach more favorable than the ones that would take into account the two experimental facts discussed above is that now we have only one parameter to tune, instead of one for the finite thickness and one for the screening.

The lower part of Fig. 12 shows the single-particle occupations in the determinant. The right-most one corresponds to MDD, and there all spins are up and occupy LLL states with $l = 0, 1, \dots, 5$. In the left-most configuration, electrons fill the two lowest shell of $B = 0$. The logic of the configurations between these two extremes is that the occupation is moving towards LLL. The second configuration is obtained from the first one by flipping one spin and moving it to LLL. The reason behind having $S = 1$ is the exchange energy, and only secondly the energy lowering by the Zeeman term. In the third configuration, the electrons are already on the LLL, and this state corresponds to the $\nu = 2$ IQHE state. As B increases, the electrons start to flip spins one by one, until the configuration is the fully spin-polarized $\nu = 1$ state. One can see that the determinant part of the wave function is here given by Eq. (12). These determinants have a CM motion in the ground state. In some cases that have more than one important non-interacting configuration present in the interacting case, one can still transform it to a single-configuration one by a coordinate transformation $\mathbf{r} \rightarrow \mathbf{r} - \mathbf{r}_{\text{cm}}$ ²⁴. This is done only on the phase part of the wave function, as the exponential part is always the same and corresponds to the correct ground state of the CM motion. This coordinate transformation has an important consequence, namely that after this is done, every single-particle wave function in the determinant depends on all electron coordinates via \mathbf{r}_{cm} . In practice, this means that the commonly used computational rules for the determinant ratios are not trivially applicable anymore. For this reason, it might be better to move all the electrons at the same time.

It is relatively easy to find the relevant single-particle configurations,

Variational Monte Carlo for Interacting Electrons in Quantum Dots

like the ones shown above in Fig. 12. For a weak B , the configurations reflect the shell structure of the $B = 0$ case where Hund's rules can be used as an initial guideline. When one moves to higher B values, the total angular momentum gets larger. The energies plotted in Fig. 1 give some idea of various possibilities for the configurations. One should also note that it is rather trivial to test various configurations in VMC, as the simulations are very fast. In addition, even the energies with rather large statistical error are accurate enough to tell if one should pay any attention to the configuration in question.

One should note that in this regime, also the mean-field theories might work in a reasonable fashion in most cases. The density-functional theory predictions are compared with the those of VMC in Refs. 25 and 26. The cases where mean-field theory breaks down are typically such that there are several important configurations in the ground state. Another minor problem of the mean-field results is that the relative accuracy depends on the total spin of the system²⁶.

3.4. Fractional Quantum Hall Effect Regime

The FQHE regime starts at the reconstruction of the MDD state. The important difference, as pointed out above, is that in the FQHE regime, the interactions start to dominate. At IQHE cases the phase structure is still very well approximated by a single Slater determinant, but for the FQHE limit, the many-body wave functions have phase structures that are fundamentally of a many-body nature. The rather accurate Laughlin states are among the few exceptions¹². These wave functions for QD's can be written as

$$\Psi(\mathbf{r}_1, \mathbf{r}_2, \dots, \mathbf{r}_N) = \exp \left[- \sum_{i=1}^N r_i^2 / 2 \right] \prod_{i < j}^N z_{ij}^m, \quad (34)$$

with only one letter (m , needs to be odd) difference to the MDD state, see Eq. (13). Actually, MDD is obtained with $m = 1$ and those with $m = 3, 5, \dots$ really correspond to a FQHE case. The FQHE filling factor in these states is $\nu = 1/m$. If one splits the MDD-part from the Laughlin states, the remaining factor $\prod_{i < j}^N z_{ij}^{m-1}$ can be thought as a generalized two-body Jastrow factor.

One can multiply the Laughlin wave function by a traditional Jastrow factor, and lower the energy. One can thus split the correlation effects into two parts, the one on the LLL and the one that takes into account the higher Landau levels. We call the second part of the correlation effects Landau-level mixing (LLM). For three electrons, a particle number that is still rather accurately solved by the exact diagonalization, VMC results show

A. Harju

that 96-98% of the LLM effects on the energy are captured by the simple two-body Jastrow factor²⁷.

It turns out that the LLL part in the correlation is far more complicated. The two-electron case is, of course, a simple exception, as the LLL wave functions are easily found from Eq. (29). But for larger particle numbers, no simple routes to exact wave functions have been found. The LLL wave function of fully spin polarized cases in the FQHE regime can be written as

$$\Psi(\mathbf{r}_1, \mathbf{r}_2, \dots, \mathbf{r}_N) = \exp \left[- \sum_{i=1}^N r_i^2 / 2 \right] \prod_{i < j}^N z_{ij} P_{\Delta L} , \quad (35)$$

where $P_{\Delta L}$ is a symmetric polynomial of degree ΔL of all the variables $\{z_i\}_{i=1}^N$. The wave function is thus the MDD one multiplied by a polynomial. The task is to find the coefficients of this polynomial. If $\Delta L = 1$, the polynomial is a trivial sum

$$S_1 = \sum_{i=1}^N z_i , \quad (36)$$

which can easily be seen to correspond to an excitation of the CM motion, as $S_1 = N z_{\text{cm}}$. The case of $\Delta L = 2$ is also easy to find, if one writes it as a polynomial that is orthogonal to S_1^2 . To do this in practice, one can write any P_2 and apply a coordinate transformation (as we did in Section 3.3.) $z_i \rightarrow z_i - z_{\text{cm}}$. If the result is zero, then the initial polynomial was S_1^2 . In other cases one finds a polynomial which is

$$\tilde{S}_2 = \sum_{i_1 < i_2}^N (z_{i_1} - z_{\text{cm}})(z_{i_2} - z_{\text{cm}}) , \quad (37)$$

where the tilde on \tilde{S}_2 is used to distinguish it from the elementary symmetric polynomials

$$\begin{aligned} S_1 &= \sum_{i_1} z_{i_1} , \\ S_2 &= \sum_{i_1 < i_2} z_{i_1} z_{i_2} , \\ S_k &= \sum_{i_1 < i_2 < \dots < i_k} z_{i_1} z_{i_2} \dots z_{i_k} , \\ S_N &= z_{i_1} z_{i_2} \dots z_{i_N} . \end{aligned} \quad (38)$$

These functions can actually be used as a basis for the QD studies in the FQHE regime^{28,29}. If one is only interested in the ground states, the S_1 polynomial can be dropped from the basis, but then one has to replace z_i

Variational Monte Carlo for Interacting Electrons in Quantum Dots

by $z_i - z_{\text{cm}}$ in the higher order polynomials. We mark these polynomials by \tilde{S}_L (with $L > 1$) below.

Using the polynomials \tilde{S}_L , the problem for three electrons is rather low dimensional. The calculations show that the ground states occur at additional angular momentum values $\Delta L = 3 \times i$, where i is a positive integer²⁷. The LLL-part of the ground state with $\Delta L = 3$ is directly \tilde{S}_3 , as it is the only possibility on the given basis. One has to remember that S_1 cannot be present in ground states, as it corresponds to a CM excitation. For $\Delta L = 6$, the two polynomials in the basis are \tilde{S}_3^2 and \tilde{S}_2^3 . The polynomial \tilde{S}_3^2 is more important, it has an overlap of 0.958 with the exact state, whereas the Laughlin $m = 3$ state has an overlap of 0.991. The next ground state with $\Delta L = 9$ consists of $\tilde{S}_2^3\tilde{S}_3$ and \tilde{S}_3^3 , where the second one is more important with an overlap of 0.972 with the exact state. A similar trend continues for higher values of ΔL , and still at $\Delta L = 30$ when the full basis (using S instead of \tilde{S}) is 91 dimensional, the problem is six dimensional in the basis of \tilde{S}_L functions. Furthermore, the overlap of \tilde{S}_3^{10} with the exact state is still 0.983.

For larger particle numbers, the physics get more complicated. One can approximate the determinant part by a single determinant written in coordinates $z_i - z_{\text{cm}}$. In Fig. 13, the overlap for the $N = 5$ case is shown. One can see that the overlap decreases dramatically for large values of ΔL . For $\Delta L = 5$, one can approximate the state by a polynomial \tilde{S}_5 . For higher ΔL , more and more polynomials are needed to accurately describe the states. In spite of that, one can actually find very nice agreement for the ΔL values of the ground states using transformed determinants³⁰. One would not expect this from the overlaps shown above. The values of ΔL are not actually trivial for larger particle numbers. If one forgets the LLM and finds the possible ground states on LLL theory, exact diagonalization is a very natural tool for that¹⁶. The LLL ground states can be seen in Fig. 14, where we plot by a star each ΔL value that can be the ground state of the system of N electrons at some value of B . For $N \leq 5$, ΔL is an integer times N , but for larger particles number, more irregular behavior of ΔL is seen. The state with $\Delta L = N$ is a possible ground state for $N \leq 14$. For $N = 14$, the ground state has an overlap of 0.996 with a state with polynomial \tilde{S}_{14} . One should note that this polynomial corresponds to a case with one flux quantum through the center of mass. The state of Ref. 31 is nearly exact with an overlap of 0.99991 with the exact state. The nature of the first post-MDD state changes at $N = 12$. For $N \geq 15$ the $\Delta L = N$ is not a ground state anymore.

The composite-fermion (CF) theory is one possibility for constructing the variational wave function^{32,33}. It is, however, rather nontrivial to con-

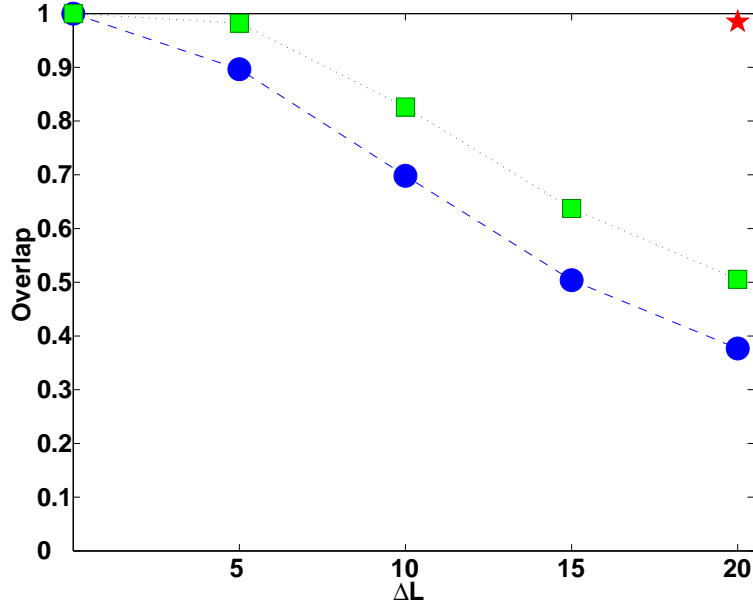


Fig. 13. Overlap of a single-determinantal wave function with the exact one as a function of the additional angular momentum ΔL for five electrons. The higher points are obtained with a coordinate transformation $z_i \rightarrow z_i - z_{\text{cm}}$, and the lower ones without it. The pentagram at $\Delta L = 20$ shows the overlap of the Laughlin $\nu = 1/3$ state.

struct a complete CF theory for all states of the QD's in the FQHE regime. Especially, one needs to go beyond the mean-field rule used in many cases to obtain the ΔL values of the CF theory³⁰. In an easy example of the CF theory, two vortices are added to each electron as

$$\prod_{i < j}^N z_{ij}^2, \quad (39)$$

and the electrons are considered to move in an effective magnetic field that is obtained from the external B by subtracting the field strength of the added vortices. If the resulting field is still reasonably strong and to the direction of the external B , the electron wave function can be taken to be, e.g., that of the MDD. Doing this, the $\nu = 1/3$ Laughlin state is obtained. If, however, the resulting effective field is again reasonably strong but this time opposite to the external B , the electrons can form the MDD for this opposite B . To obtain this, one has to transform $z_{ij} \rightarrow z_{ij}^*$ in MDD wave function. Next, one needs to project this to LLL, and one possibility is to replace z^* by a

Variational Monte Carlo for Interacting Electrons in Quantum Dots

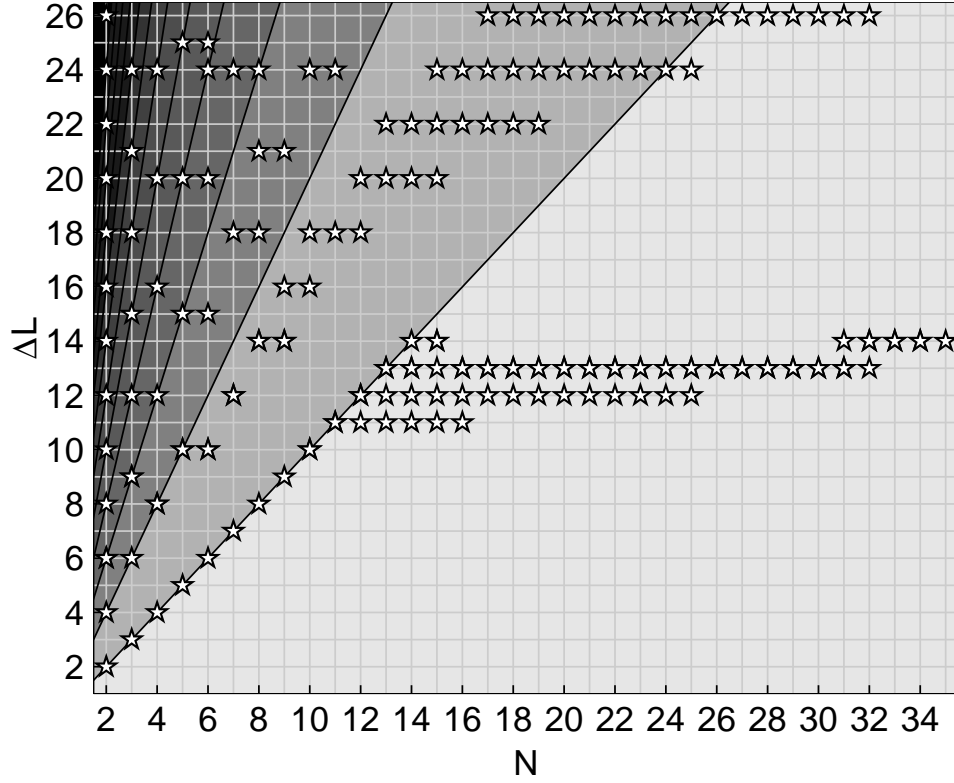


Fig. 14. Possible ground state additional angular momentum values (ΔL) for various particle numbers (N) from an exact lowest-Landau-level theory. For small N , ΔL is regular but more complicated structures are seen on larger particle numbers.

derivative $\partial/\partial z$. Thus the wave function is

$$\Psi(\mathbf{r}_1, \mathbf{r}_2, \dots, \mathbf{r}_N) = \exp \left[-\sum_{i=1}^N r_i^2/2 \right] \prod_{i < j}^N \left(\frac{\partial}{\partial z_i} - \frac{\partial}{\partial z_j} \right) \prod_{i < j}^N z_{ij}^2, \quad (40)$$

and the two products can be simplified to a simple product of MDD: $\prod z_{ij}$. A trivial way to find this is to note that MDD is the only LLL state with the given angular momentum, and that each derivative lowers the angular momentum of $\prod z_{ij}^2$ by one. These two examples are the limiting ones, and there are other possibilities in between³³. The wave functions of the electrons moving in effective fields can be as complicated as the ones of the original problem. In addition, the projection used above is not the only possibility. An interesting finding using CF theory is that one can obtain more accurate

A. Harju

states than the Laughlin $\nu = 1/3$ one by calculating

$$\Psi(\mathbf{r}_1, \mathbf{r}_2, \dots, \mathbf{r}_N) = \exp \left[-\sum_{i=1}^N r_i^2/2 \right] \prod_{i<j}^N \left(\frac{\partial}{\partial z_i} - \frac{\partial}{\partial z_j} \right) \prod_{i<j}^N z_{ij}^4 . \quad (41)$$

This means that it is energetically favorable to add four vortices to each electron and move on a field that is opposite to the original one than to add two vortices and have an effective field that is pointing to same direction than the original field. In addition to Ref. 32, one can find see more details in Ref. 33.

An interesting question is how the LLM affects the LLL part of the wave function. In other words, if one finds first the polynomial of Eq. (35) on LLL theory, the important question is how much do the optimal coefficients change when one inserts the Jastrow correlation factor in the wave function. A possible method to answer this is the Monte Carlo -based diagonalization (MCD)²⁹. The method is similar to the exact diagonalization, but the expansion is done on a correlated basis. This means that the expansion converges faster than the one done on the non-interacting configurations. One can find rather simple form for the Hamiltonian matrix elements, namely

$$h_{ij} = \left\langle P_i^* P_j \times \left\{ \frac{1}{2}(E_i + E_j) + V_I + \frac{1}{2} \left| \frac{\nabla J}{J} \right|^2 \right\} \right\rangle_{|\Psi_0 J|^2} , \quad (42)$$

where configurations \mathbf{R} are sampled from $|\Psi_0 J|^2$, and in our case, Ψ_0 is MDD, P 's are the symmetric polynomials, V_I is the interaction and impurity potential, and energies E_i and E_j are found from

$$\mathcal{H}_0 \Psi_0 P_i = E_i \Psi_0 P_i . \quad (43)$$

The overlap matrix elements are

$$s_{ij} = \langle P_i^* P_j \rangle_{|\Psi_0 J|^2} , \quad (44)$$

and the Schrödinger equation is given in a matrix form as

$$\mathbf{H}\boldsymbol{\alpha} = E\mathbf{S}\boldsymbol{\alpha} . \quad (45)$$

The reason to use Monte Carlo for the matrix elements is that the integrals needed are high-dimensional. By the MCD method, one obtains, in addition to the ground states, also the excited states.

As an example of the accuracy of the method, the interaction energies of six fermions and bosons are shown in Fig. 15. The data is obtained from a few-minute runs, and the maximum error in the LLL is 0.0004 for

Variational Monte Carlo for Interacting Electrons in Quantum Dots

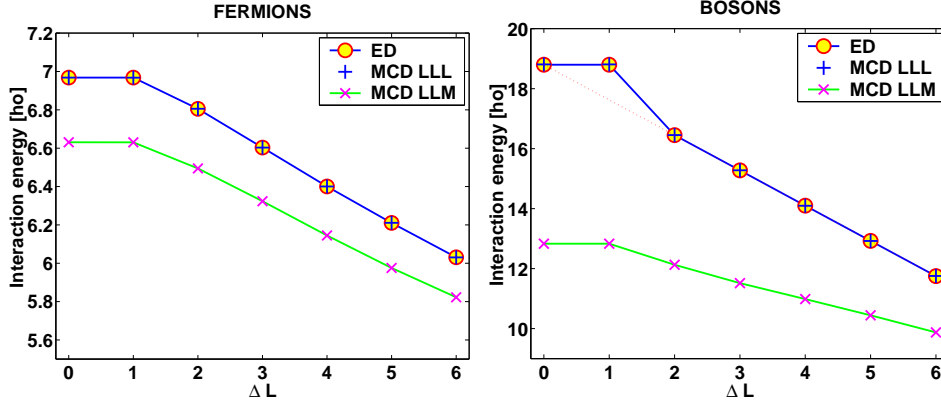


Fig. 15. Interaction energy (in units of $\hbar\omega$) for six fermions and bosons as a function of the additional angular momentum. For LLL, MCD is compared with the exact numbers, and perfect agreement is found. The LLM energy shows the energy lowering by the Jastrow factor.

fermions and 0.01 for bosons. The energy lowering obtained by adding the Jastrow factor is significant. It is larger for bosons because they lack the Pauli principle that keeps the spin-polarized electrons of the fermion case further apart already on the LLL.

A very interesting feature of the MCD method is that any classical potential is easy to add. To demonstrate this, we have added a point-charge impurity to the $N = 6$ QD. The resulting electron density is shown in Fig. 16. One can see that the left side of the density in Fig. 16(a) still looks flat like the one of MDD, but when the magnetic field gets stronger, electrons start to localize, see Fig. 16(b). One can clearly see the six peaks in density corresponding to the electrons in the system. More details of MCD can be found from Ref. 35.

Finally, there is also a possibility to find partially spin polarized states after MDD³⁴. Of course, this depends crucially on the strength of the Zeeman coupling to spin. For realistic parameters of the GaAs QD's, the $N = 6$ QD has a ground state with one flipped spin after the MDD state. Here the LLL approximation has rather different phase diagram of post-MDD states than the one with higher levels also via the Jastrow factor, see Fig. 17.

4. CONCLUSIONS

We have constructed a variational wave function for quantum dots in various magnetic field regimes. The variational quantum Monte Carlo

A. Harju

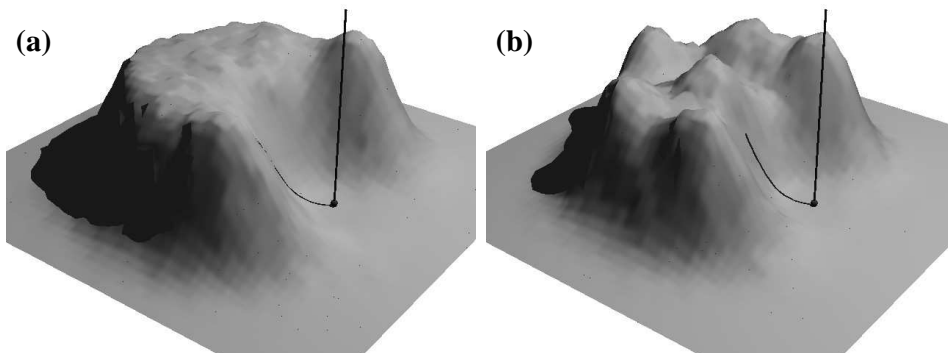


Fig. 16. The charge density of a six-electron GaAs quantum dot, with a point-like impurity on the plane of the electrons (indicated by the line segment). The external confinement is $\hbar\omega = 3$ meV and the magnetic field is 4 T in (a) and 6 T in (b). Particles start to localize at stronger magnetic field.

method has shown to be accurate for all magnetic fields. The simple single configuration Slater-Jastrow wave function can be used for many cases, the possible exceptions being some of the states found in the extreme magnetic fields where the system is in the fractional quantum Hall effect regime. In this limit, we show that it is possible to tailor a new type of a quantum Monte Carlo method that naturally includes the multi-configurational nature of the system.

ACKNOWLEDGMENTS

I would like to thank (in alphabetic order) Matti Alatalo, Bernardo Barbiellini, Veikko Halonen, Petteri Hyvönen, Karri Niemelä, Martti Puska, Stephanie Reimann, Henri Saarikoski, Sami Siljamäki, Juha Suorsa, and Viktor Sverdlov for collaboration and Sigridur Sif Gylfadottir, Meri Helle (née Marlo), Risto Nieminen, and Esa Räsänen also for their careful reading of the manuscript. This research is supported by the Finnish Academy of Science and Letters and the Academy of Finland, partly via its Centers of Excellence Program (2000-2005).

REFERENCES

1. S.M. Reimann and M. Manninen, *Rev. Mod. Phys.* **74**, 1283 (2002).

Variational Monte Carlo for Interacting Electrons in Quantum Dots

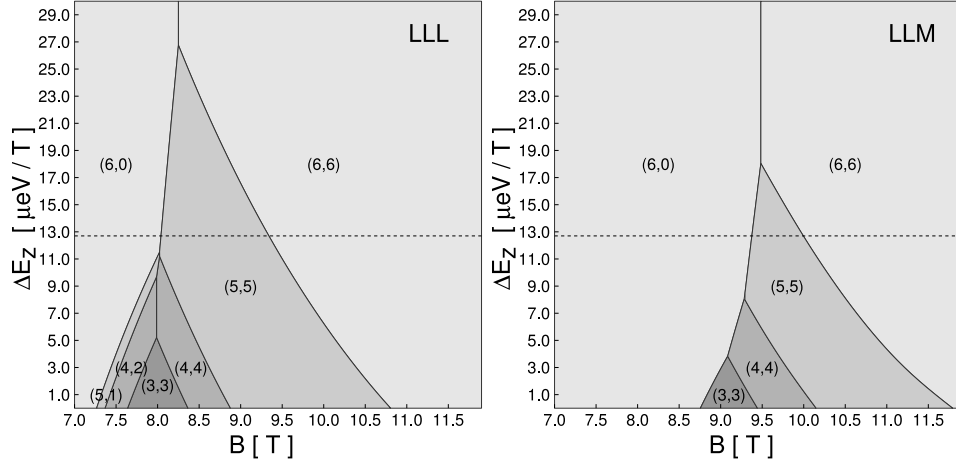


Fig. 17. Phase diagrams for six electrons in the lowest Landau level approximation (left panel) and with Landau-level mixing (right panel). The labeling of the states is: $N_{\uparrow}, \Delta L$, where N_{\uparrow} is the number of spin-up electrons and ΔL is the additional angular momentum ($L_{\text{MDD}} = 15$ for six electrons). The vertical axis is the strength of the Zeeman coupling per spin, $\Delta E_z = |\frac{1}{2}\mu_B g^*|$, the value of which in GaAs ($12.7 \mu\text{eV/T}$) is marked by dashed lines in the figures. Other parameters are: $m^*/m_0 = 0.067$, $\hbar\omega_0 = 5 \text{ meV}$ and $\epsilon_r = 12.4$. The relative interaction strength C varies from 1.23 ($B = 7 \text{ T}$) to 1.01 ($B = 12 \text{ T}$).

2. W.M.C. Foulkes, L. Mitas, R.J. Needs, and G. Rajagopal, *Rev. Mod. Phys.* **73**, 33 (2001).
3. G. Ortiz, D.M. Ceperley, and R.M. Martin, *Phys. Rev. Lett.* **71**, 2777 (1993).
4. V. Fock, *Z. Phys.* **47**, 446 (1928).
5. E. Räsänen, A. Harju, M. J. Puska, and R. M. Nieminen, *Phys. Rev. B* **69**, 165309 (2004).
6. A.H. MacDonald, S.-R. Eric Yang, and M.D. Johnson, *Aust. J. Phys.* **46**, 345 (1993).
7. F. Bolton, *Ph.D. Thesis*, Universität Regensburg, 1994.
8. F. Pederiva, C.J. Umrigar, and E. Lipparini, *Phys. Rev. B* **62**, 8120-8125 (2000); Erratum *ibid.* **68**, 089901 (2003).
9. M. Marlo, A. Harju, and R.M. Nieminen, *Phys. Rev. Lett.* **91**, 187401 (2003).
10. M. Marlo-Helle, A. Harju, and R.M. Nieminen, *Physica E* **26**, 286 (2005).
11. P. Nightingale, private discussion.
12. R.B. Laughlin in *The Quantum Hall effect*, ed. by R.E. Prange and S.M. Girvin (Springer-Verlag, New York, 1987), p. 233.
13. X. Lin, H. Zhang, A.M. Rappe, *J. Chem. Phys.* **112**, 2650 (2000).
14. A. Harju, B. Barbiellini, S. Siljamäki, R.M. Nieminen and G. Ortiz, *Phys. Rev. Lett.* **79**, 1173 (1997).
15. A. Harju, B. Barbiellini, R.M. Nieminen, and V.A. Sverdlov, *Physica B* **255**,

A. Harju

- 145 (1998).
16. H. Saarikoski, A. Harju, M.J. Puska, R.M. Nieminen, *Phys. Rev. Lett.* **93**, 116802 (2004).
 17. H. Saarikoski, A. Harju, M.J. Puska, R.M. Nieminen, *Physica E* **26**, 317 (2005).
 18. H. Saarikoski, S.M. Reimann, E. Räsänen, A. Harju, and M.J. Puska, *Phys. Rev. B* **71**, 035421 (2005).
 19. A. Harju, S. Siljamäki, and R.M. Nieminen, *Phys. Rev. Lett.* **88**, 226804 (2002).
 20. M. Marlo, M. Alatalo, A. Harju, and R.M. Nieminen, *Phys. Rev. B* **66**, 155322 (2002).
 21. A. Harju, S. Siljamäki, and R.M. Nieminen, *Phys. Rev. B* **65**, 075309 (2002).
 22. E. Räsänen, H. Saarikoski, V.N. Stavrou, A. Harju, M.J. Puska, and R.M. Nieminen, *Phys. Rev. B* **67**, 235307 (2003).
 23. A. Harju, E. Räsänen, H. Saarikoski, M.J. Puska, R.M. Nieminen, and K. Niemelä, *Phys. Rev. B* **69**, 153101 (2004).
 24. A. Harju, V.A. Sverdlov, R.M. Nieminen, and V. Halonen, *Phys. Rev. B* **59**, 5622 (1999).
 25. H. Saarikoski, E. Räsänen, S. Siljamäki, A. Harju, M.J. Puska, and R.M. Nieminen, *Eur. Phys. J. B* **26**, 241 (2002).
 26. H. Saarikoski, E. Räsänen, S. Siljamäki, A. Harju, R.M. Nieminen, and M.J. Puska, *Phys. Rev. B* **67**, 205327 (2003).
 27. A. Harju, V. A. Sverdlov, and R.M. Nieminen, *Europhys. Lett.* **41**, 407 (1998).
 28. S. Siljamäki, V. Sverdlov, A. Harju, P. Hyvönen, and R. Nieminen, *Physica B* **284–288**, 1776 (2000).
 29. S. Siljamäki, A. Harju, E. Räsänen, J. Suorsa, R.M. Nieminen, *Physica E* **26**, 441 (2005).
 30. A. Harju, S. Siljamäki, and R.M. Nieminen, *Phys. Rev. B* **60**, 1807 (1999).
 31. J.H. Oaknin, L. Martín-Moreno, J.J. Palacios, and C. Tejedor, *Phys. Rev. Lett.* **74**, 5120 (1995).
 32. J.K. Jain and R.K. Kamilla, *Int. J. Mod. Phys. B* **11**, 2621 (1997).
 33. S. Siljamäki, *M.Sc. Thesis*, Helsinki University of Technology, 1999.
 34. S. Siljamäki, A. Harju, V. Sverdlov, P. Hyvönen, and R. Nieminen, *Phys. Rev. B* **65**, 121306(R) (2002).
 35. S. Siljamäki, *Dr. Thesis*, Helsinki University of Technology, 2003. (Available at <http://lib.hut.fi/Diss/2003/isbn9512267047/>)